

## Different Binding Modes of Structurally Diverse Ligands for Human D3DAR

Gabriella Ortore,\* Tiziano Tuccinardi, Elisabetta Orlandini, and Adriano Martinelli

Dipartimento di Scienze Farmaceutiche, Università di Pisa, via Bonanno 6, 56126 Pisa, Italy

Received July 28, 2010

Five different dopamine D3 receptors (D3DARs) models were created considering some suggested binding modes for D3DAR antagonists reported in earlier computational studies. Different hypotheses are justified because of the lack of experimental information about the putative site of interaction and are also due to the variability in scaffolds and size of D3DAR ligands. In this study 114 potent and selective D3DAR antagonists or partial agonists are used as key experimental information to discriminate the most reliable receptor model and to build a docking based 3D quantitative structure–activity relationship model able to indicate the ligand properties and the residues important for activity. The ability of this D3DAR model to discriminate the binding mode of different classes of ligands, showing a good quantitative correlation with their activity, encourages us to use it for screening novel lead compounds.

### INTRODUCTION

Dopamine D3 receptors (D3DARs) are already recognized drug targets in the treatment of Parkinson's disease<sup>1</sup> and schizophrenia<sup>2,3</sup> and have emerged in the past few years as potential targets in substance abuse.<sup>4,5</sup> Compared with other dopamine receptor subtypes, D3DARs have lower incidence and are mainly postsynaptically located in the nucleus accumbens and in the island of Calleja,<sup>6</sup> which are associated with emotional and cognitive functions.<sup>7</sup> This localization evokes an involvement in the defective functioning in schizophrenia<sup>8</sup> and in the drug use. Recent studies on acute and chronic drug taking<sup>9</sup> have revealed that the simple stimulation of dopamine receptors to produce pleasure is only an initiating factor in drug abuse, but the correlated process is very unclear. It is well-known that ligands targeting dopamine receptors nonselectively would have limited therapeutic use in the treatment of drug abuse,<sup>10</sup> such as for cocaine, one of the most abused drugs for which there is no medication available, because of their untoward side effects. Furthermore, the potential of dopaminergic agonists in drug addiction has not shown to be promising in clinical trials for drug abuse.<sup>11</sup> Therefore, considerable efforts are involved in the ongoing search for potent and selective D3DAR partial agonists and antagonists, which recently led to the identification of many structurally unrelated compounds.<sup>4,12–14</sup>

Only two distinct structural features are common among all of the D3DAR antagonists: an amino group with lipophilic substituents and at least one aryl moiety. The second generation of D3DAR-selective antagonists and partial agonists also presents an alkyl spacer taking an amide, heteroatom, or heterocycle, which might possibly enable hydrogen bonding. Antagonists based on aminotetralin,<sup>15–17</sup> tetrahydroisoquinoline,<sup>18,19</sup> benzazepine,<sup>20–23</sup> aminoindane<sup>24</sup> derivatives, pyrrolidine<sup>25</sup> and pyrrole<sup>26</sup> scaffolds, and 4-phenylpiperazine<sup>5,27</sup> compounds all share these features (see Chart 1).

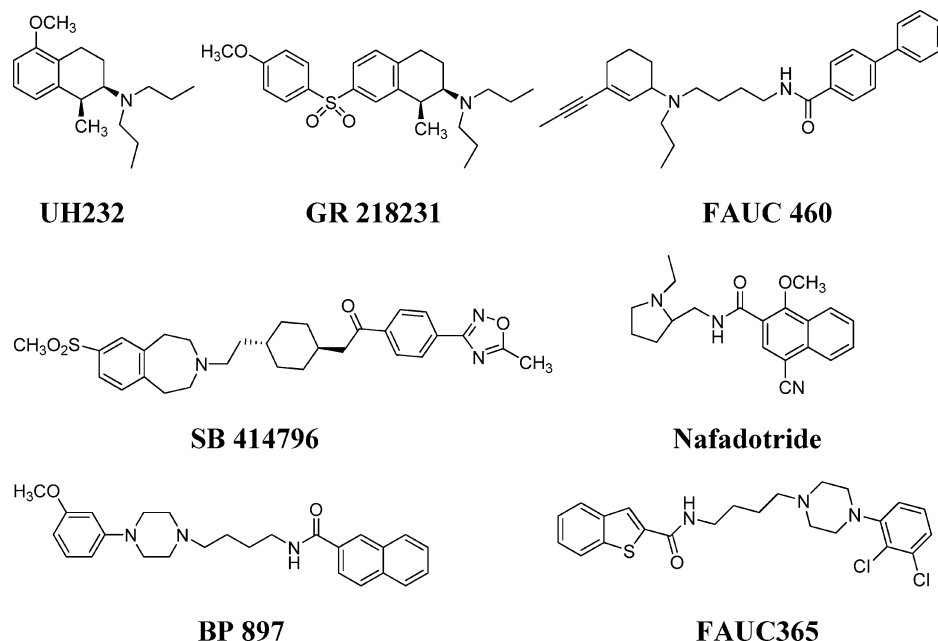
All these categories of compounds contain ligands of very different sizes, ranging from about 15 to 40 heavy atoms. The high diversity within the scaffold of D3DAR-selective antagonists or partial agonists, in the absence of a crystallographic structure of the receptor, makes a theoretical investigation on their binding affinity extremely difficult. Nevertheless, since many of these D3DAR ligands show high activity and selectivity, they can be used for the construction of receptor models as a useful tool for gaining deeper insight into ligand–receptor interactions and for quickly screening novel lead compounds with high affinities toward D3DAR. Some authors have performed molecular modeling studies on D3DARs and have hypothesized different binding modes in the transmembrane (TM) arrangement for spiperone,<sup>28</sup> 7OH-DPAT,<sup>29</sup> two hexahydropyrazinoquinoline derivatives,<sup>30</sup> *N*-(7-(4-(2-methoxyphenyl)piperazin-1-yl)bicyclo[3.3.0]-octane-3-yl)-2-naphthalenecarboxamide,<sup>27</sup> and benzazepine derivatives.<sup>31</sup> These discrepancies are justified because of the lack of experimental information about the putative site of interaction, like an adequate amount of mutational data performed with structurally different dopamine ligands, or the substituted cysteine accessibility method (SCAM) results.

In order to further investigate the structural details of the interactions between D3DAR and the very different molecular scaffolds of selective ligands with antagonist or partial agonist activity, we performed a receptor modeling and automated docking study on the D3 subtype, starting from the different binding modes already hypothesized in literature.

### RESULTS AND DISCUSSION

**Molecular Modeling of D3DAR.** We started the modeling of human D3DAR using the crystallographic structure of bovine rhodopsin (RHO) as a template.<sup>32</sup> The successive crystallization of  $\beta_2$  and  $\beta_1$  adrenergic and A2a adenosine receptors provided new insights into their molecular arrangements but seemed not to contribute significant variations in the homology models, due to the remarkable similarity of the overall structures of rhodopsin, adrenergic, and adenosine

\* Corresponding author. E-mail: ortore@farm.unipi.it. Telephone: +39-050-2219572.

**Chart 1.** Structures of Some Potent D3DAR Antagonists or Partial Agonists

receptors.<sup>33–35</sup> Thus, we used the RHO-based model of D3DAR for the subsequent docking studies.

The sequence alignment of RHO and the dopaminergic receptor subtypes (Figure S1, Supporting Information) was generated through the PRALINE program<sup>36</sup> with a low gap penalty, using all the dopamine receptors subtypes. The alignment is consistent with the one reported in our previous work on D2 and D4 subtypes<sup>37</sup> and is also in agreement with the findings of previous sequence analysis studies. The highly conserved residues for all the dopaminergic receptors and also the positions which appear to be important for the folding of the helices or for the receptor activation are aligned (see Figure S1, Supporting Information). The homology between D3DAR and the template exceeds 40% in the transmembrane region. There is no alignment for the third dopaminergic intracellular loop (IL), much longer than that of bovine rhodopsin, but it was irrelevant for the purpose of this study because it was found to have no effect on ligand binding in previous studies on chimeric receptors.<sup>38</sup>

The three-dimensional model of D3DAR was generated using the MODELLER program,<sup>39</sup> on the basis of the alignment reported in Figure S1, Supporting Information, refined by means of molecular mechanics (MM) and molecular dynamics (MD) calculations and checked with PROCHECK<sup>40</sup> (see the Experimental Section for details). The Ramachandran plot of the D3DAR model (Figure 1) showed five residues in disallowed regions, three localized in the loops and two in the TMs borders, far away from the binding site, Asp5.37(187) at the beginning of TM3 and Lys396 at the end of TM8.

The model was refined through 1 ns of MD simulation using the AMBER program<sup>41</sup> in a fully hydrated phospholipid bilayer environment made up of dipalmitoylphosphatidylcholine (DPPC) molecules solvated by TIP3 water molecules, as described in the Experimental Section. The stability of the model was evaluated by calculating the root-mean-square deviation (rmsd) of all the heavy atoms of the TM helices along the trajectory (see Figure 1), from the

starting D3DAR model structure; in the last 600 ps an equilibrate structure was achieved.

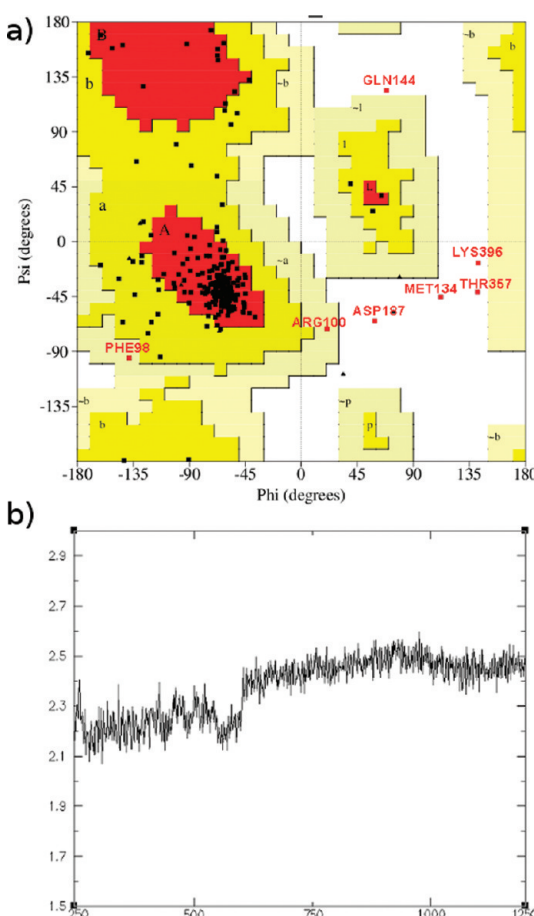


**Figure 1.** Ramachandran plot of the D3DAR model (a). The most favored regions are colored in red, additional allowed, generously allowed and disallowed regions are indicated as yellow, light-yellow, and white, respectively. The heavy atoms rmsd from the starting structures obtained after heating and equilibration of the D3DAR (b) as a function of simulation time at 300 K.

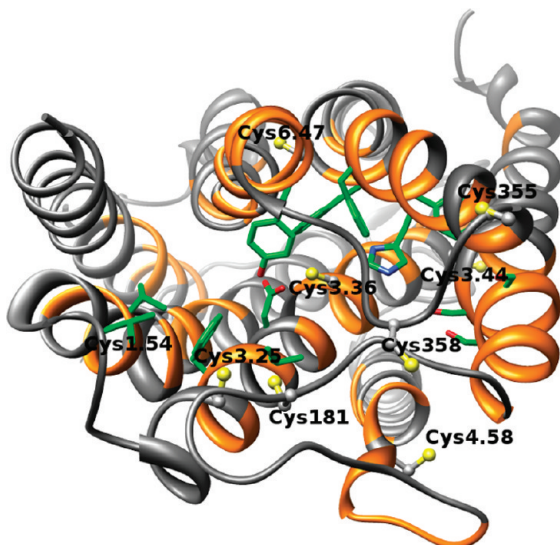


**Figure 2.** SCAM reactive residues (orange ribbon), cysteines (ball and stick represented), and residues considered as involved in the ligand binding at D2DAR (green, stick represented) in our D3DAR model.

In order to validate the D3DAR molecular model,<sup>42</sup> the refined structure of the receptor was compared with the experimental data reported in literature for the dopaminergic receptors. The high homology between the D2 and D3 subtypes in the TM region (about 80%) enabled us to use the SCAM results for the D3 receptor and then to consider as water exposed the D3DAR residues corresponding in the alignment with the same positions of the D2DAR SCAM-reactive aminoacids.<sup>43–50</sup>

Thus, we checked the arrangement of TMs and found that the positions aligned with the D2DAR methanethiosulfonate-reactive residues were situated in our model at the internal surface of the transmembrane crevice (see Figure 2) or in the extracellular face of the receptor and thus exposed to the solvent. Only some residues were not in agreement with the SCAM results, as already described for D2DAR.<sup>37</sup>

Other site-directed mutagenesis studies suggested some residues as critical for the ligand affinity in the dopamine receptors: (i) Asp3.32(110), responsible for a strong ionic bond with a cationic protonatable amine moiety on dopaminergic ligands, (ii) Ser5.42, 5.43, and 5.46, whose hydrogen-bond network orients ligands in the binding site, and (iii) W6.48, F6.51, F6.52, and H6.55, which are probably responsible for the receptor activation through a steric clash between their aromatic moieties and the aromatic portion of the ligands.<sup>51–58</sup> All these residues, like the amino acids corresponding to the ones responsible for D2DAR/D4DAR selectivity, are enclosed in the region around D3.32(110) (see Figure 2), except for Ser5.43(193), which is believed to be not directly involved in the binding with the ligands. In particular, for D3DAR a site-directed mutagenesis study suggested that the role of Ser5.42(192) was dominant for the binding of dopamine and 7-OH-DPAT with respect to the other serines.<sup>59</sup>

Furthermore, some G protein-coupled receptors (GPCRs) are believed to be held in the inactive state through an ionic bond between Asp3.49, Glu6.30, and Arg3.50 and to alter the configuration of the TM6 pro-kink during the activation, allowing a movement of TM6 away from TM3 through a

modulation of Cys6.47 and Trp6.48.<sup>60</sup> In particular, some authors hypothesized that Cys6.47t/Trp6.48g+/Phe6.52g+ represents the inactive conformation of the receptor, while Cys6.47g+/Trp6.48t/Phe6.52t represents the active state.<sup>61</sup> The ionic bond network present in our model between Asp3.49(127), Arg3.50(128), and Glu6.30(324) and the rotamer positions of Cys6.47(341) and Trp6.48(342) was consistent with the hypothesized inactive conformation of the receptor.

Unfortunately, scarce information is available on residues specifically involved in the D3DAR binding with antagonists,<sup>62</sup> so it is difficult to identify the binding site region and to validate the three-dimensional structure of the receptor on the basis of experimental data suggesting the ligand–receptor interactions. Some results of a mutagenesis study carried out on D3DAR/D1DAR transmembrane chimeras,<sup>63</sup> using test ligands of various chemical templates, proposed that each D3DAR TM segment disproportionately contributes to receptor ligand interactions, with a general order of decreasing impact, like TM7, TM3 > TM4 > TM6 > TM5. In particular it seemed to be perturbed only a specific microbinding region in a given chimera using different radioactive ligands, supporting the hypothesis that the affinity changes arise from alterations in different critical binding domains for particular ligands, rather than from nonspecific effects on receptor conformation. For example, benzamide antagonists, like raclopride, showed a marked affinity decrease in D3DAR TM3, TM5, and TM7 chimeras, whether the binding of compounds, like haloperidol and spiperone, was affected from the replacement of TM3, TM4, and TM7. Unfortunately, the chimeras involving regions toward the extracellular side of TM1 could not be examined because the D3DAR/D1DAR replacement regarded only five amino acids (1.45–1.48 and 1.51), situated toward the intracellular region. Aminotetralin antagonists, like AJ-76 and UH-232, showed moderate affinity alterations with TM3, TM4, and TM7 chimeras, like also 3-PPP, which seemed, however, more influenced by the TM7 replacement. There were not any results on the binding of D3/D1DAR chimeras with 4-phenylpiperazine compounds, the last generation of D3DAR-selective antagonists.

The most reliable and recurrent experimental information about the D3DAR is just the receptor affinity data.<sup>4,7,15–44</sup> Unfortunately, the binding assays on these compounds were performed with many different radioligands, and their results are not at all comparable.

Therefore, our gain was to use a set of D3DAR antagonists or partial agonists affinities, obtained with similar experimental procedures, to further validate our receptor model using a 3D-QSAR analysis.

**Docking of FAUC365 and Modeling of Complexes.** As the three-dimensional structure of our D3DAR model was consistent with the D2DAR SCAM results and with the putative dopamine binding site arrangement proposed in literature, we used this model to carry out a four-step computational procedure: (i) construction of the complexes **a–e** (Figure 3), with different plausible orientations of a selective D3DAR ligand in the TMs region, (ii) refinement of the complexes through a molecular dynamics and mechanics simulation, (iii) screening of 114 D3DAR ligands in each of the hypothetical refined complexes through molecular docking, and (iv) 3D-QSAR analysis of these

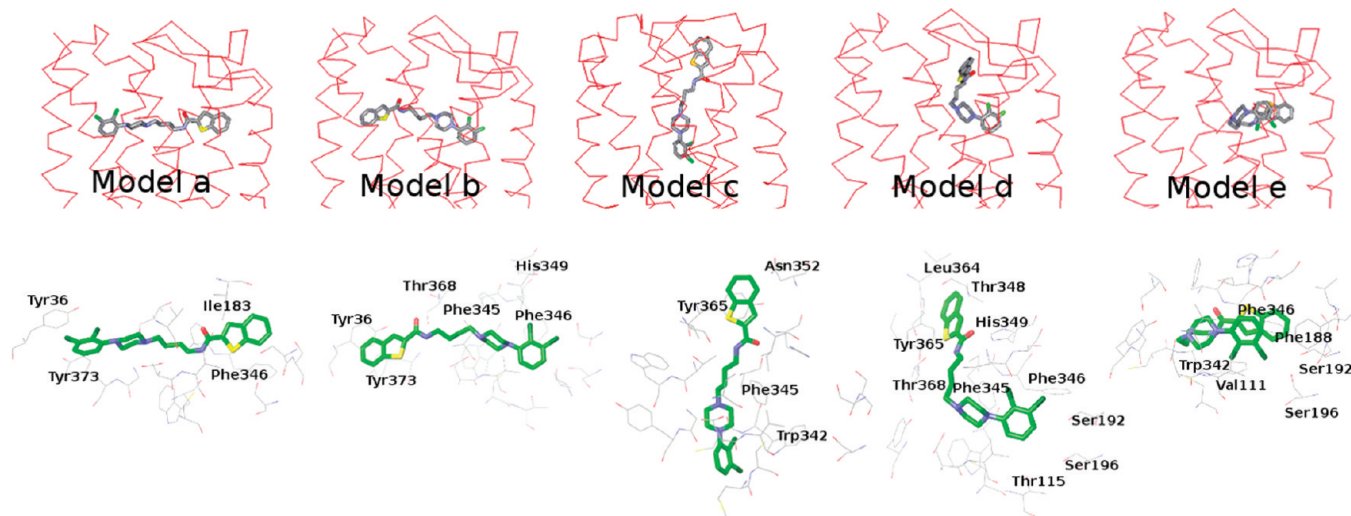


**Figure 3.** Possible binding modes of FAUC365 in D3DAR suggested from some previously reported computational studies, here used as a starting point for the receptor modeling of models **a–e** (up), and the respective binding sites arrangement after MD simulation (down).

**Table 1.** Main Interactions of FAUC365's Fragment A, B, and Amido Group in the Binding Site of Models **a–e**

| fragment       | A  | B                                      | NH-C=O         |
|----------------|--|--|----------------|
| Model <b>a</b> | Tyr36, Tyr373                                  | Ser192, Ser196, Phe345, Phe346, His349 | —              |
| Model <b>b</b> | Phe346   | Tyr36, Tyr373                          | Thr368         |
| Model <b>c</b> | Trp342   | Tyr365                                 | —              |
| Model <b>d</b> | Cys114, Thr115, Ser192, Ser196, Phe345, Phe346 | Thr348, Leu364, Tyr365                 | His349, Thr368 |
| Model <b>e</b> | Val111, Phe188                                 | Trp342, Phe346                         | —              |

ligands in the orientation of the best docking pose, in order to choose the best model and the most plausible binding site arrangement.

We choose FAUC365,<sup>64</sup> one of the most selective D3DAR antagonists of the new generation with subnanomolar affinity for this receptor, to construct five hypothetical complexes, inserting the ligand in such a way that the strong ionic bond between Asp3.32(110) and the cationic protonatable amine moiety of the ligand was preserved. In the assembly we took into account some hypotheses about the binding modes of D3DAR antagonists arising from previously reported computational studies, considering FAUC365 in the anti conformation, and positioning this ligand in such a way that its functional groups could engage interactions similar to the ones visualized for each hypothesized binding mode in the reference article.<sup>28,30,65</sup> The **a** and **b** orientations filled the whole hypothetical binding site, from TM1 to TM5, as suggested by Ding et al. for their hexahydropyrazinoquinoline derivatives,<sup>30</sup> and by Boeckler et al. for spiperone,<sup>28</sup> and Ehrlich et al. for their phenylpiperazines,<sup>65</sup> respectively. The **c** orientation was longitudinal in the receptor crevice, in a similar manner to the *N*-(*ω*-(4-(2-methoxyphenyl)piperazin-1-yl)alkyl)carboxamides reported by Hackling et al.<sup>27</sup> In complex **d** a half ligand occupies the region between Asp3.32(110) and Ser5.42(192), and the other one points toward the extracellular loops, in analogy with the L-shaped docking proposed for some fused benzazepines by the GlaxoSmithKline researchers.<sup>31</sup> Finally, model **e** takes into account the preferred conformation of a series of piperazinylalkylisoxazole analogues analyzed by Cha et al. in a comparative molecular field analysis (CoMFA) study<sup>66</sup> also reported as U-shaped docking conformation for some triazole thiopropyl tetrahydrobenzazepines;<sup>21</sup> the collapsed conformation allows the insertion of the whole ligand between

Asp3.32(110) and Ser5.42(192), because of the large size of the cavity. The five ligand–receptor complexes were refined through MD simulations, using the procedure described in the Experimental Section.

At the end of MD simulation (see Figure 3), all the compounds preserved the hydrogen bond between the piperidine protonated nitrogen and Asp3.32(110). The main interactions engaged by the dichlorophenyl ring (A), the benzothiophene moiety (B), and the amido group with the binding site residues of each receptor model are schematized in Table 1. Nevertheless the spacer and the amido benzothiophene occupy the same region in both **c** and **d** complexes, the side chains of His6.55(349), Thr7.38(368), and in particular Tyr7.35(365) rearranged their conformation in order to adapt the binding site to the ligand in the two different orientations. This produces a shift of the amido benzothiophene toward the inner part of the receptor in complex **d** and promotes a further hydrogen bonding with Thr7.38(368).

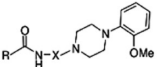
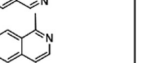
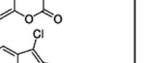
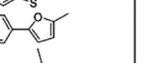
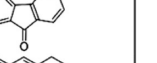
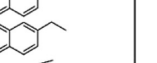
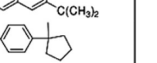
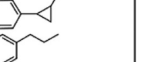
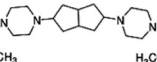
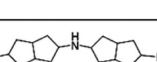
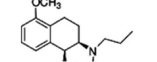
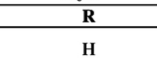
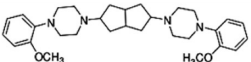
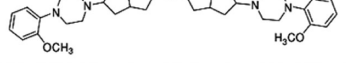
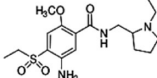
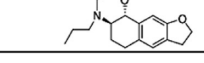
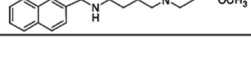
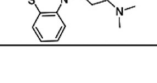
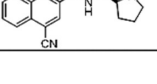
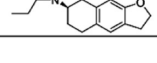
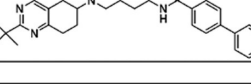
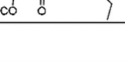
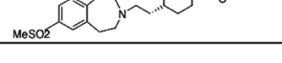
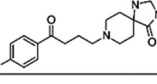
In model **e** the collapsed ligand insertion in this binding site provokes a rearrangement of the aromatic microdomain (His6.55, Phe6.51, Phe6.52, and Trp6.48) probably responsible for the receptor activation; in particular a critical conformational change of Trp6.48 toward a trans-conformation was detected.

**Docking of Known Ligands.** We use our five possible arrangements of D3DAR with FAUC365 to perform an automated docking. We utilized the GOLD program<sup>67</sup> to produce the most plausible dopaminergic complexes for the ligands reported in Table 2, all D3DAR antagonists or partial agonists with different affinity profiles for the D3 subtype, tested using [<sup>125</sup>I]iodosulpride as a radioligand. These compounds shared their capability to inhibit D3DARs with a common therapeutic target as the treatment of drug

**Table 2.** Structures, Experimental and Predicted Affinities of Compounds 1–114

| Compound <sup>15</sup>     | R1                                | R2           | Exp           | Calcd      |       |       |
|----------------------------|-----------------------------------|--------------|---------------|------------|-------|-------|
| 1                          | OMe                               | Me           | 7.9           | 7.71       |       |       |
| 2                          | OH                                | Me           | 8.6           | 7.82       |       |       |
| 3                          | OMe                               | Pr           | 9.1           | 8.73       |       |       |
| 4                          | OH                                | Pr           | 9.7           | 8.72       |       |       |
| 5                          | H                                 | Pr           | 8.8           | 8.73       |       |       |
| 6 <sup>a</sup>             | Cl                                | Pr           | 8.8           | 8.86       |       |       |
| 7                          | Br                                | Pr           | 8.9           | 8.76       |       |       |
| 8                          | CN                                | Pr           | 9.3           | 8.60       |       |       |
| 9 <sup>a</sup>             | CONH <sub>2</sub>                 | Pr           | 8.4           | 8.14       |       |       |
| 10                         | OSO <sub>2</sub> Me               | Pr           | 8.9           | 8.59       |       |       |
| 11 <sup>a</sup>            | OSO <sub>2</sub> CF <sub>3</sub>  | Pr           | 8.8           | 8.43       |       |       |
|                            |                                   |              |               |            |       |       |
| Compound <sup>16</sup>     | R1                                | R2           | n             | Stereoc    | Exp   | Calcd |
| 12                         | H                                 | H            | 2             | trans      | 7.8   | 8.01  |
| 13                         | H                                 | H            | 2             | cis        | 6.6   | 7.25  |
| 14 <sup>a</sup>            | MsO                               | H            | 2             | cis        | 6.6   | 6.66  |
| 15 <sup>a</sup>            | MeO                               | H            | 2             | (S,S)trans | 8.1   | 8.48  |
| 16                         | OH                                | H            | 2             | (S,S)trans | 9     | 8.59  |
| 17                         | MsO                               | H            | 2             | (S,S)trans | 8.2   | 8.43  |
| 18                         | MeO                               | H            | 2             | (R,R)trans | 6.1   | 6.31  |
| 19 <sup>a</sup>            | OH                                | H            | 2             | (R,R)trans | 6.2   | 6.30  |
| 20                         | MsO                               | H            | 2             | (R,R)trans | 5.9   | 6.35  |
| 21                         | H                                 | H            | 1             | trans      | 7.8   | 7.94  |
| 22                         | H                                 | H            | 1             | cis        | 7.3   | 7.63  |
| 23                         | MeO                               | H            | 1             | trans      | 7.8   | 8.47  |
| 24 <sup>a</sup>            | OH                                | H            | 1             | trans      | 8.7   | 7.94  |
| 25                         | MsO                               | H            | 1             | trans      | 8.3   | 8.57  |
| 26                         | H                                 | OH           | 2             | trans      | 8.1   | 8.67  |
| 27                         | H                                 | MsO          | 2             | trans      | 6.7   | 7.70  |
| 28                         | H                                 | OH           | 1             | trans      | 7.9   | 7.67  |
| 29 <sup>a</sup>            | H                                 | MsO          | 1             | trans      | 7.3   | 8.19  |
|                            |                                   |              |               |            |       |       |
| Compound <sup>26</sup>     | R                                 | X            | Stereoc       | Exp        | Calcd |       |
| 30                         | H                                 |              | trans         | 6.9        | 7.55  |       |
| 31                         | 8-OCH <sub>3</sub>                |              | trans         | 7.1        | 7.89  |       |
| 32                         | 8-F                               |              | trans         | 8.1        | 7.66  |       |
| 33                         | 8-Cl                              |              | trans         | 7.8        | 7.84  |       |
| 34 <sup>a</sup>            | 8-Br                              |              | trans         | 7.8        | 7.85  |       |
| 35                         | 7-OCH <sub>3</sub>                |              | trans         | 7.1        | 7.42  |       |
| 36 <sup>a</sup>            | 8-CN                              |              | (3aR,<br>9bS) | 8.6        | 7.86  |       |
| 37                         | 7-CN                              |              | trans         | 7.6        | 7.95  |       |
| 38 <sup>a</sup>            | 8-CN                              |              | (3aR,<br>9bS) | 8.0        | 8.12  |       |
| 39                         | 8-CN                              |              | (3aR,<br>9bS) | 9.0        | 8.04  |       |
| 40 (S33084) <sup>a</sup>   | 8-CN                              |              | (3aR,<br>9bS) | 9.5        | 8.72  |       |
| 41                         | 8-CN                              |              | (3aR,<br>9bS) | 9.7        | 8.74  |       |
| 42                         | 8-Br                              |              | cis           | 7.0        | 7.23  |       |
| 43                         | 8-CN                              |              | cis           | 7.0        | 6.68  |       |
|                            |                                   |              |               |            |       |       |
| Compound <sup>23</sup>     | R                                 | Exp          | Calcd         |            |       |       |
| 44 <sup>a</sup>            | 4-Quinolyl                        | 7.6          | 7.43          |            |       |       |
| 45                         | 1-Naphthyl                        | 7.7          | 7.60          |            |       |       |
| 46                         | 5-Quinolyl                        | 7.9          | 7.54          |            |       |       |
| 47                         | 2-Indolyl                         | 7.8          | 8.05          |            |       |       |
| 48                         | 2-Naphthyl                        | 7.7          | 8.00          |            |       |       |
| 49                         |                                   | 8.0          | 7.83          |            |       |       |
|                            |                                   |              |               |            |       |       |
| Compound <sup>23</sup>     | R                                 | Exp          | Calcd         |            |       |       |
| 50                         |                                   | 8.2          | 7.89          |            |       |       |
| 51                         |                                   | 8.2          | 8.14          |            |       |       |
| 52 <sup>a</sup>            |                                   | 8.2          | 8.19          |            |       |       |
| 53 <sup>a</sup>            |                                   | 8.0          | 8.18          |            |       |       |
| 54 <sup>a</sup>            |                                   | 8.5          | 8.04          |            |       |       |
| 55                         |                                   | 8.4          | 8.45          |            |       |       |
| 56                         |                                   | 8.5          | 8.44          |            |       |       |
| 57                         |                                   | 8.4          | 8.21          |            |       |       |
|                            |                                   |              |               |            |       |       |
| Compound <sup>18</sup>     | R                                 | Exp          | Calcd         |            |       |       |
| 58 <sup>a</sup>            | CF <sub>3</sub> SO <sub>2</sub> O | 8.4          | 8.55          |            |       |       |
| 59 <sup>a</sup>            | NC                                | 7.9          | 8.70          |            |       |       |
|                            |                                   |              |               |            |       |       |
| Compound <sup>18</sup>     | R1                                | R2           | Exp           | Calcd      |       |       |
| 60 <sup>a</sup>            | 7-CN                              |              | 8.9           | 8.87       |       |       |
| 61                         | 7-CN                              |              | 8.5           | 8.02       |       |       |
| 62                         | 7-CN                              |              | 8.7           | 8.43       |       |       |
| 63                         | 6-CN                              |              | 7.8           | 8.14       |       |       |
| 64                         | 6-CN                              |              | 8.5           | 7.91       |       |       |
| 65                         | 6-CN                              |              | 8.3           | 7.84       |       |       |
| 66                         | 6-CN                              |              | 8.5           | 7.74       |       |       |
| 67                         | 6-CN                              | 2-naphthyl   | 8.0           | 8.26       |       |       |
| 68                         | 6-CN                              | 1-naphthyl   | 8.1           | 8.55       |       |       |
| 69 (SB277011) <sup>a</sup> | 6-CN                              | 4-quinolinyl | 8.0           | 7.35       |       |       |
|                            |                                   |              |               |            |       |       |
| Compound <sup>27</sup>     | R                                 | X            | Exp           | Calcd      |       |       |
| 70 <sup>a</sup>            |                                   |              | 6.1           | 6.91       |       |       |
| 71                         |                                   |              | 7.0           | 6.73       |       |       |
| 72 <sup>a</sup>            |                                   |              | 7.4           | 6.70       |       |       |
| 73                         |                                   |              | 7.4           | 7.41       |       |       |
| 74                         |                                   |              | 6.5           | 6.84       |       |       |
| 75 <sup>a</sup>            |                                   |              | 9.3           | 8.72       |       |       |
| 76                         |                                   |              | 8.4           | 8.13       |       |       |
| 77                         |                                   |              | 6.4           | 7.05       |       |       |
| 78                         |                                   |              | 9.0           | 8.65       |       |       |
| 79                         |                                   |              | 8.1           | 8.32       |       |       |
| 80 <sup>a</sup>            |                                   |              | 8.6           | 7.83       |       |       |
| 81                         |                                   |              | 8.6           | 8.84       |       |       |
| 82                         |                                   |              | 8.0           | 8.02       |       |       |
|                            |                                   |              |               |            |       |       |

Table 2. Continued

| Compound <sup>27</sup>                | R   | X                               | Exp  | Calcd |  |  |
|---------------------------------------|---|---------------------------------|------|-------|--|--|
| 83                                    |      | (CH <sub>2</sub> ) <sub>3</sub> | 6.5  | 6.79  |  |  |
| 84                                    |      | (CH <sub>2</sub> ) <sub>4</sub> | 8.1  | 7.83  |  |  |
| 85                                    |      | (CH <sub>2</sub> ) <sub>3</sub> | 6.7  | 7.04  |  |  |
| 86                                    |      | (CH <sub>2</sub> ) <sub>4</sub> | 8.2  | 9.00  |  |  |
| 87                                    |      | (CH <sub>2</sub> ) <sub>4</sub> | 8.8  | 8.82  |  |  |
| 88                                    |      | (CH <sub>2</sub> ) <sub>4</sub> | 8.0  | 7.89  |  |  |
| 89                                    |      | (CH <sub>2</sub> ) <sub>4</sub> | 8.5  | 8.80  |  |  |
| 90 <sup>a</sup>                       |      | (CH <sub>2</sub> ) <sub>4</sub> | 8.7  | 8.93  |  |  |
| 91 <sup>a</sup>                       |      | (CH <sub>2</sub> ) <sub>4</sub> | 8.2  | 8.43  |  |  |
| 92                                    |      | (CH <sub>2</sub> ) <sub>4</sub> | 8.2  | 8.76  |  |  |
| 93                                    |      | (CH <sub>2</sub> ) <sub>4</sub> | 8.5  | 8.44  |  |  |
| 94                                    |     | (CH <sub>2</sub> ) <sub>4</sub> | 7.5  | 7.83  |  |  |
| 95                                    |    | (CH <sub>2</sub> ) <sub>3</sub> | 6.9  | 6.98  |  |  |
| 96 <sup>a</sup>                       |    | (CH <sub>2</sub> ) <sub>3</sub> | 7.0  | 7.52  |  |  |
| 97                                    |    | (CH <sub>2</sub> ) <sub>3</sub> | 6.6  | 6.64  |  |  |
| 98                                    |    | (CH <sub>2</sub> ) <sub>4</sub> | 7.4  | 7.29  |  |  |
| 99                                    |    | (CH <sub>2</sub> ) <sub>4</sub> | 7.8  | 8.04  |  |  |
| 100                                   |    | (CH <sub>2</sub> ) <sub>4</sub> | 8.3  | 8.55  |  |  |
| 101 <sup>27</sup>                     |    |                                 | 6.2  | 6.35  |  |  |
| 102 <sup>27,a</sup>                   |    |                                 | 6.5  | 7.01  |  |  |
| 103 <sup>70</sup><br>(AJ76)           | R   | H                               | 7.16 | 6.65  |  |  |
| 104 <sup>70,a</sup><br>(UH232)        | n-Pr  |                                 | 8.04 | 6.82  |  |  |
| 105 <sup>68</sup><br>(Amisulpride)    |    |                                 | 8.5  | 7.93  |  |  |
| 106 <sup>71,a</sup>                   |     |                                 | 8.0  | 8.02  |  |  |
| 107 <sup>5</sup><br>(BP 897)          |     |                                 | 9.04 | 8.81  |  |  |
| 108 <sup>96</sup><br>(Chlorpromazine) |    |                                 | 8.52 | 8.41  |  |  |
| 109 <sup>25,a</sup><br>(Nafadotride)  |    |                                 | 9.51 | 8.16  |  |  |
| 110 <sup>71</sup><br>(S14297)         |    |                                 | 7.9  | 7.77  |  |  |
| 111 <sup>17</sup>                     |    |                                 | 7.9  | 8.42  |  |  |
| 112 <sup>96</sup><br>(Sulpiride)      |  |                                 | 8.1  | 8.4   |  |  |
| 113 <sup>22,a</sup><br>(SB414796)     |   |                                 | 8.4  | 8.5   |  |  |
| 114 <sup>70</sup><br>(Spirerone)      |  |                                 | 9.21 | 9.6   |  |  |

<sup>a</sup> Compounds of the external test set.

addiction and prevention of relapse and their consistence with the rhodopsin-derived model, which corresponds to the inactive conformation of the receptor.

We generated the GOLD binding cavity of 10 Å around the ligand as a center, in such a way as to enclose all the residues suggested by literature. We performed an automated docking of FAUC365, in order to test the GOLD procedure (see the Experimental Section) and its ability to reproduce the binding geometry of FAUC365 obtained by means of the MD procedure. In order to give priority to the involvement of Asp3.32(110) in binding with ligands, we applied a constraint the formation of the hydrogen bond between

the protonated piperidine nitrogen and the carboxylic oxygen of the aspartate. This constraint is unnecessary for docking in model **a-d**, where the interaction with Asp3.32(110) is retained after the free calculation, but it is required in model **e** to allow this experimental evidence. Furthermore, to guarantee a certain plasticity of the binding site, we chose some protein residues to be treated as flexible, in particular the key residues resulting from mutagenesis studies and some others capable of hydrogen bonding the ligands. We explored the rotamer variability of Asp3.32(110), Ser5.42(192), Ser5.46(196), His6.55(349), and Thr7.38(368) suggested by the GOLD rotamer library.

GOLD results reproduced the orientation of FAUC365 at the end of MD simulation, with an rmsd evaluated over all the heavy atoms of the ligand of 1.2, 0.77, 0.78, 0.90, and 2.4 Å (due to the 180° rotation of the dichlorophenyl ring) in the **a–e** orientations, respectively. Thus we carried out the automated docking of the 114 ligands reported in Table 2 using the same binding site and the same GOLD parameters used for performing the FAUC365 self-test docking. The best binding poses of the ligands into models **a–e** were used as an alignment tool for the development of 3D-QSAR studies, in order to determine which of the five models is the most reliable one, with the most plausible binding site arrangement, and to further validate the receptor structure. Furthermore, a predictive 3D-QSAR model is potentially applicable toward the design of new potent D3DAR ligands.

Figure 4 shows, as an example of compounds structurally diverse from FAUC365, the orientation of amisulpride,<sup>68</sup> SB414796<sup>22</sup> and S14297,<sup>69</sup> all D3DAR selective ligands with different structures and sizes, into models **a–e**. All the models, except for the **c** model, allow a similar docking of the smaller ligands, like amisulpride and S14297; these compounds occupy the region between Asp3.49(127) and the TM5 serines. In complex **c** the GOLD program calculated for all the compounds, also for the smallest one, a longitudinal orientation, filling the central cavity of the receptor. The docking calculations cannot find the collapsed conformation as a binding mode in model **e**, where the ligands assume various orientations exploring quite different regions of the binding site, without any significant interaction. In this way, the CoMFA results proposed by Cha et al. based on their ligand-based study cannot be confirmed through the docking in our D3DAR model.

In detail, we reported the description of some representative compounds (see Figure 4), which summarizes the behavior of the antagonists or partial agonists considered in this study. For example, amisulpride engages strong hydrogen bonds with Ser5.42(192) through its sulfonyl group in models **a** (where also Ser5.46(196) is involved in a further analogues interaction), **b**, **d**, and **e** in addition to the ionic bond between Asp3.32(110) and the protonated nitrogen of the ligand. In model **c**, the sulfonyl group directs toward the extracellular side and interacts with Tyr7.35(365) and Asn6.58(352), while the aniline N engages a hydrogen bond with His6.55(349). Also in this case, the ionic bond between Asp3.49(127) and the protonated amine is retained.

The very long compound SB414796 assumes a similar arrangement in models **a** and **b**, which guarantees the interaction with Asp3.32(110), Tyr1.39(36), Ser5.42(192), and Ser5.46(196). The difference in phenyloxadiazole moiety orientation led in model **a** to the interaction of Ser5.42(192) and Ser5.46(196) with the amidic C=O and of Ser5.43(193) with the phenyloxadiazole, while in model **b** the only interaction between Ser5.42(192) and the phenyloxadiazole is detectable. These analogies between the docking poses in both models **a** and **b** are typical only for longer compounds, while molecules like BP897,<sup>5</sup> spiperone,<sup>70</sup> and FAUC365 (as in Figure 3) show a reversed arrangement in models **a** and **b**. In model **c** the main interaction of SB414796, apart from the usual ionic bond with Asp3.32(110), regards the phenyloxadiazole moiety; an aromatic stacking between Tyr7.35(365) and the phenyl and a hydrogen bond between Asn6.58(352) and the oxadiazole stabilize the longitudinal

pose in the receptor. Surely, the best stabilization of SB414796 is due to model **d**; polar interactions between Ser5.46(196) and the sulfonyl group, Asp3.32(110) and the protonated amine, and Thr7.38(368) and His6.55(349) and the aminic group contribute to the binding energy of the ligand. Furthermore, Ile183, Phe6.51(345), and Tyr7.35(365) surround the cyclohexyl ring of SB414796 in a lipophilic cavity. In model **e**, instead of the expected collapsed conformation, SB414796 assumes a “L shaped” conformation in the binding site, orienting one branch (the sulfonyl group) between TM6 and TM7 and the second one between TM5 and TM6. In this way, the oxadiazole ring lies outside of the receptor backbone, and only the ionic interaction with Asp3.32(110) is retained.

Very interesting is the D3DAR biological profile of smaller compounds like AJ76, UH232, compound **106**,<sup>71</sup> and S14297 reported in Figure 4 as an example, which shows good affinity at D3DAR despite the very different structure if compared with the new generation antagonists or the partial agonists, like BP879 or FAUC365. They occupy the same region in models **a**, **b**, **d**, and **e**, allowing a weak interaction with one of the TM5 serines in models **a**, **b**, and **d**, in addition to the hydrogen bond with Thr3.37(115) in this last model. In model **c**, the longitudinal pose cannot allow any significant interaction with the receptor, except for the constrained ionic bond with Asp3.32(110).

Analyzing the docking results, we can suppose that models **c** and **e** are worse at rationalizing the affinity of the D3DAR antagonists and the partial agonists here described, since no significant interactions between ligand and receptor were detected. Furthermore, models **a**, **b**, and especially **d** verified the involvement of TM3, TM5, and TM7 in the binding with benzamide antagonists, like amisulpride, and aminotetralin derivatives, like S14297, whether the influence of TM5 was less remarkable for compounds like FAUC365 and spiperone. This is in agreement with the studies on D3DAR/D1DAR transmembrane chimeras.<sup>63</sup>

A comparison between our results and the theoretical studies reported in literature<sup>29,66,72–74</sup> shows a generally good agreement of the binding site arrangement. In particular, the docking orientation of small compounds, like UH232 (**104**) or S14297 (**110**), proposed by Varady et al.<sup>73</sup> is reproduced in our D3DAR model, but compounds longer than haloperidol were not considered in their reported docking results. Zhao et al. showed the orientation of longer compounds,<sup>72</sup> which is similar to the binding mode in model **b**, but all these compounds were D3DAR agonists, so the models are not comparable.

**3D-QSAR Study and Models Validation.** In order to analyze the five constructed models and validate them on the basis of the available experimental data, that is the ligands affinities at D3DAR, we carried out a 3D-QSAR study on our 114 D3DAR antagonists or partial agonists, using the best docking poses in each model as receptor-based alignments. This step of the computational procedure is very helpful to choose the best model and the most plausible binding site arrangement. The activities of the data set ligands have been evaluated through binding assays using [<sup>125</sup>I]iodosulpiride in CHO cells expressing D3DARs, as reported in the Table 2 references.<sup>5,15–18,22,23,25–27,68,70,71,96</sup> The GRID/GOLPE approach<sup>75</sup> was used to define five 3D-QSAR models, using the combination of C3 (corresponding to an

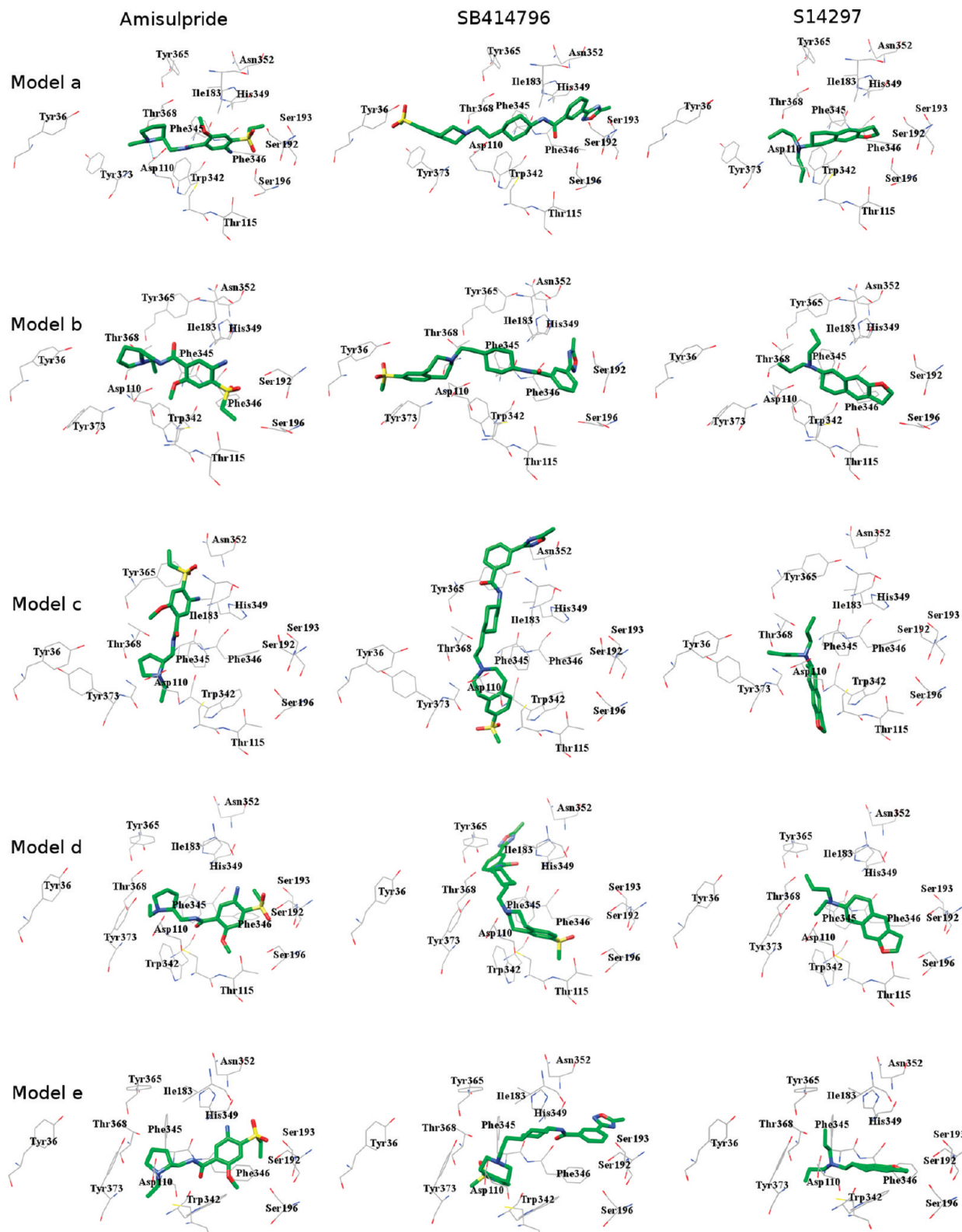


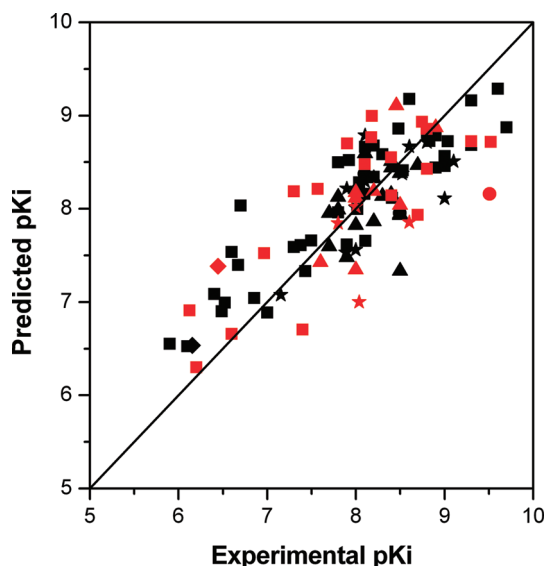
**Figure 4.** Docking of amisulpride, SB414796 and S14297, as an example of the possible binding modes of the 114 tested compounds in the five models **a–e**.

aliphatic carbon), N2 (corresponding to neutral flat NH<sub>2</sub>), and O (corresponding to a carbonyl oxygen) probes. After a test with different probes, these were the better ones for describing the molecular diversity of the training set. A further 3D-QSAR model (model BS) was developed using the best docking pose among the five previously selected to allow for different compounds adopting different orientations

in the receptor. The six 3D-QSAR models were characterized by correlation coefficient ( $r^2$ ) and predictive correlation coefficient ( $q^2$ ) values, calculated using the cross-validation routine with five random sets of compounds, for a training set of 82 compounds. Furthermore, standard deviation of errors of prediction (SDEP) was calculated for an external test set of 32 compounds.

**Table 3.** Statistical Results of the Five Receptor-Based 3D-QSAR Models **a–e** without Any Pretreatment

|          | PC | $r^2$ | $q^2$ | SDEP <sub>TS</sub> |
|----------|----|-------|-------|--------------------|
| <b>a</b> | 4  | 0.91  | 0.03  | —                  |
| <b>b</b> | 5  | 0.95  | 0.08  | —                  |
| <b>c</b> | 3  | 0.85  | -0.03 | —                  |
| <b>d</b> | 5  | 0.96  | 0.53  | 0.58               |
| <b>e</b> | 4  | 0.88  | -0.26 | —                  |
| SB       | 4  | 0.82  | -0.25 | —                  |

**Figure 5.** Plot of the 3D-QSAR results for D3DAR model **d**, experimental/predicted pIC<sub>50</sub> is reported. The training and test sets are black and red colored, respectively. The ligands are represented on the basis of their chemical structure: (■) FAUC365-like; (▲) SB414796-like; (●) sulpiride-like; (★) small ligands, S14297-like; and (◆) dimers, c101 and c102.

As reported in Table 3, the  $r^2$  values confirm that models **c** and **e** are characterized by a minor capability to correlate the ligand structures with their binding affinity. Model BS showed the worst profile, probably due to the high influence of the different binding site composition in the score calculation. A deeper analysis of the docking scores, in fact, shows that the extent of the first pose fitness is comparable only for models **a** and **b**, whose binding site is quite the same, whether there is a big difference if compared with models **c–e**, which are made by other amino acids. This difference in the binding site residues, and not only in their conformations, did not allow a realistic comparison of the docking scores among the diverse models. Without any pretreatment, among the six 3D-QSAR models, only the one obtained from model **d** presented a good predictive profile ( $q^2$  values of 0.53, SDEP<sub>TS</sub> = 0.58). After fractional factorial design (FFD) selections, this 3D-QSAR model was characterized by a  $r^2$  value of 0.96, a  $q^2$  value of 0.77, and a SDEP value of 0.62 for the prediction of the external test set.

Figure 5 shows the prediction of the D3DAR data sets binding affinities calculated through the 3D-QSAR model **d**. These results indicate that the 3D-QSAR model is able to rationalize the affinity of the D3DAR antagonists and the partial agonists here reported, quite independently from their chemical structure, and that it should be suitable for the design of new D3DAR ligands.

One important feature of 3D-QSAR analysis is graphical model representation, which is used to make interpretation

easier. In the GOLPE program, there are several options for displaying the final model. Among these, the partial least squares (PLS) pseudocoeficient plots are very useful since they make it possible to visualize favorable and unfavorable interactions between the probes and the molecules under study. Since the alignment of the ligands was performed using the structures docked into D3DAR, identification of matching alignments between the receptor and the 3D-QSAR maps was conducted, for highlighting the residues that play the most important role in the interaction. Figure 6 illustrates the negative (cyan) and positive (yellow) regions of C3, N2, and O probes of the PLS coefficients plots superimposed on the D3DAR binding site.

In the region near Thr7.38(368), a negative region in the three PLS coefficient plots indicates that a favorable interaction between a ligand and the C3 probe results in a decrease in activity, while a favorable interaction between a ligand and the N2 and O probes leads to an increase in activity. It is important to highlight that the flexibility of the Thr7.38(368) side chain led to different spatial orientations of the ligand functional groups interacting with this residue in the molecular docking and then to molecular interaction fields (MIFs) not strictly overlapped in the PLS coefficient plots. Also the negative region above Thr3.37(115) in the C3 and O PLS coefficient plots shows that in this region a favorable interaction between a ligand and the O probe or an unfavorable interaction between a ligand and the C3 probe led to an increase in activity.

The center of the lipophilic cavity defined by Val3.29(107), Phe6.51(345) and Phe6.52(346) corresponds in the C3 probe plot to a positive region, in which a favorable interaction between a ligand and the C3 probe results in an increase in activity, as well as in the O probe plot this area presents a negative region, where a favorable interaction between a ligand and the O probe results in a decrease in activity.

Obviously, the N2 PLS coefficient plot shows a region near Asp3.32(110) in which the interaction between the ligand and a hydrogen donor causes a loss of activity.

A small but significant negative region near His6.55(349) in the N2 plot, corresponding to a positive region in the O plot, highlights the importance of this residue as hydrogen-bond donor.

**Virtual Screening.** In order to test the reliability of our model, we tried to measure the enrichment ability of a virtual screening (VS) protocol in which the 3D-QSAR model generated by model **d** was used as filter.<sup>76</sup> Lacking a set of ligands and decoys already tested for D3DAR, we used the NCI Diversity Set Database<sup>77</sup> enriched with 31 D3DAR antagonists and partial agonists with nanomolar affinities<sup>78–83</sup> that were not used in the 3D-QSAR model generation. We submitted the 1364 NCI compounds and the 31 known D3DAR antagonists and partial agonists to the same docking protocol previously used for the training and test sets. The alignment of the best poses was used to predict the affinities of the 1395 compounds using our 3D-QSAR model. Figure 7 shows the primary statistical data for the known high-affinity compounds and the compounds filtered from the NCI database. Using a predicted  $pK_i$  of 8.4 as a threshold, approximately 81% of the known high-affinity compounds was maintained (Figure 7), filtering about 13% of the NCI database. The selection of 165 compounds from the NCI database determined an enrichment factor (EF) value of 6.7.

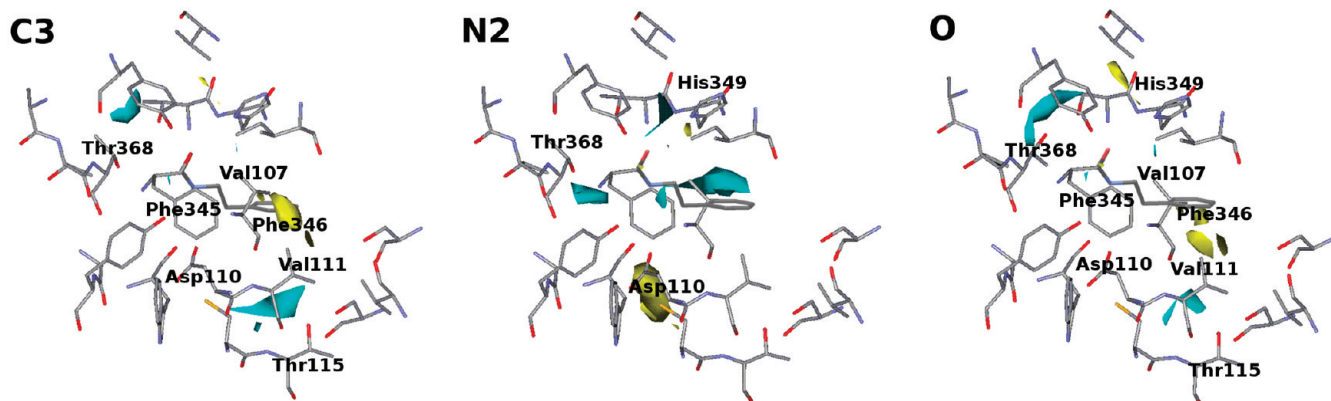


**Figure 6.** Overlap of the positive (yellow) and negative (cyan) regions for C3, N2, and O probes of the PLS coefficients plots with the D3DAR binding site.

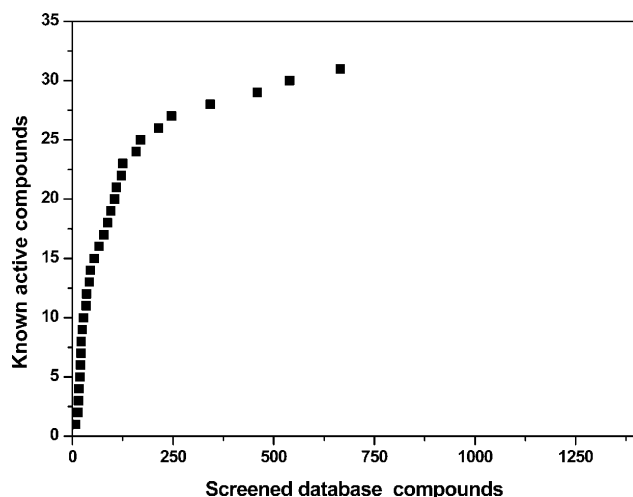


**Figure 7.** Statistical analysis of the VS study: number of filtered known compounds versus number of molecules of the database.

This value is coherent with a good procedure for a first filtering step of a virtual screening and confirmed the capability of model **d** to discriminate the D3DAR ligands.

## CONCLUSIONS

Five plausible D3DAR models, derived from different suggested dockings of antagonists in the hypothetical binding site of this receptor, were built using FAUC365 as a ligand. A graphical inspection of the five optimized complexes showed some differences in their binding site arrangement, mainly for Tyr7.43(373), and for a critical conformational change of Trp6.48 toward a trans-conformation in models **c** and **e**. The ligand position allowed in all the models the interaction with some “key residues” found in mutagenesis studies. The automated docking of 114 known D3DAR antagonists or partial agonists performed into the five models confirmed that models **c** and **e** are the worse in rationalizing the affinity of the D3DAR ligands here described, because less significant interactions between ligand and receptor are established. Furthermore, they are not compatible with some mutagenesis studies on D3DAR/D1DAR transmembrane chimeras.<sup>63</sup>

The most reliable complex, identified through a 3D-QSAR study carried out on the best docking poses of the 114 ligands into each model, seemed to be model **d**. The statistical indices  $r^2$  and  $q^2$  showed a fine correlation, and the SDEP value for

the external test set confirmed a good activity prediction. For complexes **a–c** and **e**, the predictive correlation was very poor, and these models were rejected after the first simple pretreatment. The PLS coefficient plots for model **d** highlighted the importance of His6.55(349) as a hydrogen-bond donor and Thr3.37(115) as a hydrogen-bond acceptor and of Val3.29(107), Phe6.51(345), and Phe6.52(346) surfaces as a key lipophilic interaction. Thr7.38(368), which is a nonconserved residue corresponding to a phenylalanine in D2DAR subtype, had a role as hydrogen-bond donor or acceptor. Regarding the binding mode of different classes of D3DAR ligands, model **d** allowed the disposition between Asp3.32(110) and Ser5.42(192) of smaller ligands, which are generally less selective for D3DAR. On the other hand, the antagonists of the “new generation” occupied an outer region and protruded toward the extracellular loops, interacting with His6.55(349), Tyr7.35(365), and non-conserved Thr7.38(368), apart from Asp3.32(110) and Thr3.37(115), and only weakly with the TM5 serines. The ability of this D3DAR model to discriminate the binding mode of different classes of ligands, showing a good quantitative correlation with their activity, encourages us to use it for screening novel lead compounds.

## EXPERIMENTAL

**D3DAR Modeling.** The primary sequences of dopamine receptors were retrieved from the SWISS-PROT<sup>84</sup> protein sequence database. The 3D X-ray crystallographic structure of bovine rhodopsin (1F88)<sup>85</sup> registered in the Protein Data Bank<sup>86</sup> was used as a direct template to construct the D3DAR model. The sequential alignment of all the human dopaminoergic subtypes on rhodopsin was performed by means of PRALINE,<sup>36</sup> using the Blosum series as a matrix with a gap open penalty of 15 and a gap extension penalty of 1. The incorporated PSIPRED method<sup>87</sup> was used in order to verify the presence of  $\alpha$ -helices in our TM sequence hypothesis, and the TMHMM method was chosen to predict the TM structure information. For the IL1, EL1, and EL3 loops we used the rhodopsin crystal structure as a template. The alignment of the EL2 loop on the rhodopsin one was not so good, but we used this structure as a starting point for the MD simulation because the Cys3.25–Cys181 disulfide bridge connecting the EL2 loop with TM3, which was the main structural requirement for this loop, gave a strong limitation to the conformational space. The IL3 loop was free of templates, but it was unessential for the goal of this

study and is not involved in the ligand binding.<sup>38</sup> The alignment was in agreement with previous work.<sup>28,29</sup> The numbering system suggested by Ballesteros and Weinstein was used. The most highly conserved residue in each TM helix (TMH) is assigned a value of 0.50, and this number is preceded by the TMH number and followed in parentheses by the sequence number. The other residues in the helix are given a locant value relative to this.<sup>88</sup>

The 3D model of D3DAR was constructed using the MODELLER program,<sup>39</sup> on the basis of the alignment obtained from PRALINE. The helix ends were capped with an acetyl group at the N-terminus and with an N-methyl group at the C-terminus. The receptor model was manually inserted into a previously stabilized phospholipid bilayer made up of DPPC molecules, orienting the helices of the receptor approximately parallel to the hydrocarbon chains of the phospholipids. All phospholipids within a radius of 1 Å around the receptor were deleted. MD simulations were carried out using AMBER8<sup>41</sup> with the modified parm94 force field at 300 K and an explicit solvent model TIP3P water with a 15 Å water cap. Chlorine ions were added as counterions to neutralize the system. The preliminary minimization steps and the MD simulations were performed following the procedure described by Tuccinardi et al.<sup>89</sup> MD trajectories were run using the minimized structure as a starting input, with 250 ps of heating and equilibration, followed by 1 ns of constant pressure MD, constraining all the  $\alpha$  carbons with decreasing harmonic force constant in the first 400 ps. The final structure of the receptor was obtained as the average of the last 500 ps of MD minimized with the CG method until a convergence of 0.05 kcal/Å·mol. General amber force field (GAFF) parameters were assigned to the DPPC molecules, while the partial charges were calculated using the AM1 bond charge correction (AM1-BCC) method<sup>90</sup> as implemented in the antechamber suite of AMBER8. The phospholipid bilayer system was prior stabilized by 600 ps of MD using the same parameters and procedure described elsewhere.<sup>89</sup>

The stereochemical quality of the resulting protein structure was evaluated by inspection of the  $\psi/\varphi$  Ramachandran plot obtained from PROCHECK analysis.<sup>40</sup> The MD snapshots were obtained through the PTRAJ module of AMBER8.

**Modeling of D3DAR–FAUC365 Complexes.** FAUC365 was built using the Maestro program<sup>91</sup> and subjected to a conformational search (CS) of 1000 steps in a water environment using the Macromodel program.<sup>92</sup> The Monte Carlo algorithm was used with the MMFFs force field. The ligand was then minimized using the conjugated gradient method to a convergence value of 0.05 kcal/Å·mol, using the same force field and parameters as for the CS.

Partial atomic charges from the AM1-BCC method<sup>90</sup> and AMBER atom types were assigned using the ANTECHAMBER module of AMBER8.

FAUC365 was manually docked into the D3DAR model in five different orientations, following the hypotheses previously suggested by literature for some D3DAR ligands and described in the Results and Discussion Section.<sup>21,27,28,30,31,65,66</sup>

The five resulting complexes **a–e** were submitted to a preliminary minimization in the phospholipid bilayer followed by 100 ps of heating and 1000 ps of MD, using the same parameters previously described. We applied a con-

straint on the main ligand–receptor interactions with a decreasing force constant (30, 20, 10, 1 kcal/mol) on the first 800 ps of MD, leaving the ligand free of constraints in the last 200 steps. The average structure from the last 200 ps trajectory of MD was minimized until a rms of 0.005 kcal/Å·mol was reached and used for the docking calculations.

**Docking Procedure.** Automated docking of the 114 ligands into models **a–e** was carried out by means of the GOLD 3.2 program.<sup>67</sup> The ligands were submitted to a conformational search with the same procedure already described for FAUC365. The region of interest was defined in GOLD in such a manner that it contains all the residues within 10 Å from FAUC365. The ‘allow early termination’ command was deactivated. All the ligands were submitted to 40 genetic algorithm runs using the GoldScore fitness function, clustering the output orientations on the basis of a rmsd distance of 1 Å. The default GOLD parameters were used for all the variables, except for some side chain rotamers and for the hydrogen-bond constraint between the protonated piperidine nitrogen and the carboxylic oxygen of Asp3.32. The EXTRA PARAMETER option was used to allow the side chain flexibility of Asp3.32(110), Ser5.42(192), Ser5.46(196), His6.55(349), and Thr7.38(368), suggested by the GOLD rotamer library. The best docking pose for each ligand was then used for further studies.

**3D-QSAR.** The GOLPE program<sup>75</sup> was used to define the five 3D-QSAR models, using the GRID<sup>93</sup> interaction fields as descriptors and the best docking poses as receptor-based alignments for the model.<sup>94</sup> The training set was composed of 82 compounds, characterized by affinity values spanning about 3 orders of magnitude, the minimum value of 6.2 (expressed as -log IC<sub>50</sub>) and the maximum value of 9.7. Similarly, the 32 compounds belonging to the test set showed an affinity value ranging from 6.1 to 9.5 (see Table 2).

Interaction energies between the selected probes and each molecule were calculated using a grid spacing of 1 Å. The MIFs of C3 (corresponding to a methyl group), N2 (corresponding to neutral flat NH<sub>2</sub>), and O (corresponding to an sp<sup>2</sup> carbonyl oxygen atom) probes were calculated in order to evaluate the lipophilic and hydrogen-bond donor/acceptor properties of the ligands. Variable selection was carried out by zeroing values with absolute values below 0.06 kcal/mol and by removing variables with a standard deviation below 0.1. Additionally, variables which either exhibited only two values or had a skewed distribution were also removed. The reliabilities of the 3D-QSAR models were characterized by their  $r^2$  and  $q^2$  values, calculated using the cross-validation routine with five random sets of compounds. The smart region definition (SRD) algorithm<sup>55</sup> was applied with 10% of the active variables as the number of seed (selected in the PLS weights space), a critical distance cutoff of 2.5 Å, and a collapsing distance cutoff of 4.0 Å. The groups were then used in the FFD procedure, using the cross-validation routine with five random sets of compounds.

**Virtual Screening.** The NCI diversity set,<sup>77</sup> consisting of 1364 compounds, was enriched with 31 high-affinity D3DAR antagonists and partial agonists.<sup>78–81,83</sup> These compounds were not included in the previous 3D-QSAR studies, and their affinities were tested by using [<sup>3</sup>H]-spiperone as a radioligand. Thus, we could not predict quantitatively their affinities but just considered them as high-affinity compounds. The VS results were evaluated using recall and

enrichment. The recall value for positives describes the ratio of correctly classified members of a data set and is defined by the equation  $\text{recall} = \text{tp}/(\text{tp} + \text{fn})$ , where tp is the number of high-affinity compounds not rejected (true positives), and fn is the number of high-affinity compounds rejected during the VS filtering (false negatives). The EF measures the enrichment of the method compared with random selection and is defined by equation  $\text{EF} = \text{recall} * \text{NCtot}/\text{NC}$ , where NCtot is the total number of molecules of the database (NCtot = 1364 + 31), and NC is the total number of compounds obtained at the end of the VS protocol. All graphic manipulations and visualizations were performed by means of the Maestro<sup>91</sup> and Chimera programs.<sup>95</sup>

#### ACKNOWLEDGMENT

Many thanks are due to Prof. Gabriele Cruciani and Prof. Sergio Clementi (Molecular Discovery and MIA srl) for the use of the GOLPE program in their chemometric laboratory (University of Perugia, Italy) and for having provided the GRID program.

**Supporting Information Available:** Amino acid sequence alignment of dopamine receptors and RHO generated through the PRALINE program. Structures and binding affinities of D3DAR ligands used for enriching the NCI Diversity Set. This material is available free of charge via the Internet at <http://pubs.acs.org>.

#### REFERENCES AND NOTES

- (1) Visanji, N. P.; Fox, S. H.; Johnston, T.; Reyes, G.; Millan, M. J.; Brothie, J. M. Dopamine D3 receptor stimulation underlies the development of L-DOPA-induced dyskinesia in animal models of Parkinson's disease. *Neurobiol. Dis.* **2009**, *35*, 184–92.
- (2) Bezard, E.; Ferry, S.; Mach, U.; Stark, H.; Leriche, L.; Boraud, T.; Gross, C.; Sokoloff, P. Attenuation of levodopa-induced dyskinesia by normalizing dopamine D3 receptor function. *Nat. Med.* **2003**, *9*, 762–7.
- (3) Schwartz, J. C.; Diaz, J.; Pilon, C.; Sokoloff, P. Possible implications of the dopamine D(3) receptor in schizophrenia and in antipsychotic drug actions. *Brain Res. Rev.* **2000**, *31*, 277–87.
- (4) Heidbreder, C. A.; Newman, A. H. Current perspectives on selective dopamine D(3) receptor antagonists as pharmacotherapeutics for addictions and related disorders. *Ann. N.Y. Acad. Sci.* **2010**, *1187*, 4–34.
- (5) Pilla, M.; Perachon, S.; Sautel, F.; Garrido, F.; Mann, A.; Wermuth, C. G.; Schwartz, J. C.; Everitt, B. J.; Sokoloff, P. Selective inhibition of cocaine-seeking behaviour by a partial dopamine D3 receptor agonist. *Nature* **1999**, *400*, 371–5.
- (6) Hillefors-Berglund, M.; Von Euler, G. Pharmacology of dopamine D3 receptors in the islands of Calleja of the rat using quantitative receptor autoradiography. *Eur. J. Pharmacol.* **1994**, *261*, 179–83.
- (7) Sokoloff, P.; Giros, B.; Martres, M. P.; Andrieux, M.; Besancon, R.; Pilon, C.; Bouthenet, M. L.; Souil, E.; Schwartz, J. C. Localization and function of the D3 dopamine receptor. *Arzneimittelforschung* **1992**, *42*, 224–30.
- (8) Luedtke, R. R.; Mach, R. H. Progress in developing D3 dopamine receptor ligands as potential therapeutic agents for neurological and neuropsychiatric disorders. *Curr. Pharm. Des.* **2003**, *9*, 643–71.
- (9) Volkow, N. D.; Fowler, J. S.; Wang, G. J.; Swanson, J. M. Dopamine in drug abuse and addiction: results from imaging studies and treatment implications. *Mol. Psychiatry* **2004**, *9*, 557–69.
- (10) Platt, D. M.; Rowlett, J. K.; Speelman, R. D. Behavioral effects of cocaine and dopaminergic strategies for preclinical medication development. *Psychopharmacology* **2002**, *163*, 265–82.
- (11) Grabowski, J.; Shearer, J.; Merrill, J.; Negus, S. S. Agonist-like, replacement pharmacotherapy for stimulant abuse and dependence. *Addict. Behav.* **2004**.
- (12) Hackling, A. E.; Stark, H. Dopamine D3 receptor ligands with antagonist properties. *ChemBioChem* **2002**, *3*, 946–61.
- (13) Newman, A. H.; Grundt, P.; Nader, M. A. Dopamine D3 receptor partial agonists and antagonists as potential drug abuse therapeutic agents. *J. Med. Chem.* **2005**, *48*, 3663–79.
- (14) Boeckler, F.; Gmeiner, P. Dopamine D3 receptor ligands: recent advances in the control of subtype selectivity and intrinsic activity. *Biochim. Biophys. Acta* **2007**, *1768*, 871–87.
- (15) Boyfield, I.; Coldwell, M. C.; Hadley, M. S.; Johnson, C. N.; Riley, G. J.; Scott, E. E.; Stacey, R.; Stemp, G.; Thewlis, K. M. A novel series of 2-aminotetralins with high affinity and selectivity for the dopamine D3 receptor. *Bioorg. Med. Chem. Lett.* **1997**, *7*, 1995–1998.
- (16) Avenell, K. Y.; Boyfield, I.; Coldwell, M. C.; Hadley, M. S.; Healy, M. A.; Jeffrey, P. M.; Johnson, C. N.; Nash, D. J.; Riley, G. J.; Scott, E. E.; Smith, S. A.; Stacey, R.; Stemp, G.; Thewlis, K. M. Fused aminotetralins: novel antagonists with high selectivity for the dopamine D3 receptor. *Bioorg. Med. Chem. Lett.* **1998**, *8*, 2859–64.
- (17) Avenell, K. Y.; Boyfield, I.; Hadley, M. S.; Johnson, C. N.; Nash, D. J.; Riley, G. J.; Stemp, G. Heterocyclic analogues of 2-aminotetralins with high affinity and selectivity for the dopamine D3 receptor. *Bioorg. Med. Chem. Lett.* **1999**, *9*, 2715–20.
- (18) Stemp, G.; Ashmeade, T.; Branch, C. L.; Hadley, M. S.; Hunter, A. J.; Johnson, C. N.; Nash, D. J.; Thewlis, K. M.; Vong, A. K.; Austin, N. E.; Jeffrey, P.; Avenell, K. Y.; Boyfield, I.; Hagan, J. J.; Middlemiss, D. N.; Reavill, C.; Riley, G. J.; Routledge, C.; Wood, M. Design and synthesis of trans-N-[4-[2-(6-cyano-1,2,3,4-tetrahydroisoquinolin-2-yl)ethyl]cyclohexyl]-4-quinolinecarboxamide (SB-277011): A potent and selective dopamine D(3) receptor antagonist with high oral bioavailability and CNS penetration in the rat. *J. Med. Chem.* **2000**, *43*, 1878–85.
- (19) Austin, N. E.; Avenell, K. Y.; Boyfield, I.; Branch, C. L.; Coldwell, M. C.; Hadley, M. S.; Jeffrey, P.; Johns, A.; Johnson, C. N.; Nash, D. J.; Riley, G. J.; Smith, S. A.; Stacey, R. C.; Stemp, G.; Thewlis, K. M.; Vong, A. K. Novel 1,2,3,4-tetrahydroisoquinolines with high affinity and selectivity for the dopamine D3 receptor. *Bioorg. Med. Chem. Lett.* **1999**, *9*, 179–84.
- (20) Micheli, F.; Bonanomi, G.; Braggio, S.; Capelli, A. M.; Damiani, F.; Di Fabio, R.; Donati, D.; Gentile, G.; Hamprecht, D.; Perini, O.; Petrone, M.; Tedesco, G.; Terreni, S.; Worby, A.; Heidbreder, C. New fused benzazepine as selective D3 receptor antagonists. Synthesis and biological evaluation. Part 2: [g]-fused and hetero-fused systems. *Bioorg. Med. Chem. Lett.* **2008**, *18*, 908–12.
- (21) Micheli, F.; Bonanomi, G.; Blaney, F. E.; Braggio, S.; Capelli, A. M.; Checchia, A.; Curcuruto, O.; Damiani, F.; Fabio, R. D.; Donati, D.; Gentile, G.; Gribble, A.; Hamprecht, D.; Tedesco, G.; Terreni, S.; Tarsi, L.; Lightfoot, A.; Stemp, G.; Macdonald, G.; Smith, A.; Pecoraro, M.; Petrone, M.; Perini, O.; Pineri, J.; Rossi, T.; Worby, A.; Pilla, M.; Valerio, E.; Griffante, C.; Mugnaini, M.; Wood, M.; Scott, C.; Andreoli, M.; Lacroix, L.; Schwarz, A.; Gozzi, A.; Bifone, A.; Ashby, C. R., Jr.; Hagan, J. J.; Heidbreder, C. 1,2,4-triazol-3-yl-thiopropyl-tetrahydrobenzazepines: a series of potent and selective dopamine D(3) receptor antagonists. *J. Med. Chem.* **2007**, *50*, 5076–89.
- (22) Macdonald, G. J.; Branch, C. L.; Hadley, M. S.; Johnson, C. N.; Nash, D. J.; Smith, A. B.; Stemp, G.; Thewlis, K. M.; Vong, A. K.; Austin, N. E.; Jeffrey, P.; Winborn, K. Y.; Boyfield, I.; Hagan, J. J.; Middlemiss, D. N.; Reavill, C.; Riley, G. J.; Watson, J. M.; Wood, M.; Parker, S. G.; Ashby Jr., C. R. Design and synthesis of trans-3-(2-(4-(3-(3-(5-methyl-1,2,4-oxadiazolyl))-phenyl)carboxamido)cyclohexyl)ethyl)-7-methylsulfonyl-2,3,4,5-tetrahydro-1H-3-benzazepine (SB-414796): a potent and selective dopamine D3 receptor antagonist. *J. Med. Chem.* **2003**, *46*, 4952–64.
- (23) Austin, N. E.; Avenell, K. Y.; Boyfield, I.; Branch, C. L.; Hadley, M. S.; Jeffrey, P.; Johnson, C. N.; Macdonald, G. J.; Nash, D. J.; Riley, G. J.; Smith, A. B.; Stemp, G.; Thewlis, K. M.; Vong, A. K.; Wood, M. Novel 2,3,4,5-tetrahydro-1H-3-benzazepines with high affinity and selectivity for the dopamine D3 receptor. *Bioorg. Med. Chem. Lett.* **2000**, *10*, 2553–5.
- (24) Haadsma-Svensson, S. R.; Cleek, K. A.; Dinh, D. M.; Duncan, J. N.; Haber, C. L.; Huff, R. M.; Lajiness, M. E.; Nichols, N. F.; Smith, M. W.; Svensson, K. A.; Zaya, M. J.; Carlsson, A.; Lin, C. H. Dopamine D(3) receptor antagonists. 1. Synthesis and structure-activity relationships of 5,6-dimethoxy-N-alkyl- and N-alkylaryl-substituted 2-aminoindans. *J. Med. Chem.* **2001**, *44*, 4716–32.
- (25) Sautel, F.; Griffon, N.; Sokoloff, P.; Schwartz, J. C.; Launay, C.; Simon, P.; Costentin, J.; Schoenfelder, A.; Garrido, F.; Mann, A. Nafadotride, a potent preferential dopamine D3 receptor antagonist, activates locomotion in rodents. *J. Pharmacol. Exp. Ther.* **1995**, *275*, 1239–46.
- (26) Dubuffet, T.; Newman-Tancredi, A.; Cussac, D.; Audinot, V.; Loutz, A.; Millan, M. J.; Lavielle, G. Novel benzopyrano[3,4-c]pyrrole derivatives as potent and selective dopamine D3 receptor antagonist. *Bioorg. Med. Chem. Lett.* **1999**, *9*, 2059–64.
- (27) Hackling, A.; Ghosh, R.; Perachon, S.; Mann, A.; Holtje, H. D.; Wermuth, C. G.; Schwartz, J. C.; Sippl, W.; Sokoloff, P.; Stark, H. N-(omega-(4-(2-methoxyphenyl)piperazin-1-yl)alkyl)carboxamides as dopamine D2 and D3 receptor ligands. *J. Med. Chem.* **2003**, *46*, 3883–99.

- (28) Boeckler, F.; Lanig, H.; Gmeiner, P. Modeling the similarity and divergence of dopamine D2-like receptors and identification of validated ligand-receptor complexes. *J. Med. Chem.* **2005**, *48*, 694–709.
- (29) Varady, J.; Wu, X.; Fang, X.; Min, J.; Hu, Z.; Levant, B.; Wang, S. Molecular modeling of the three-dimensional structure of dopamine 3 (D3) subtype receptor: discovery of novel and potent D3 ligands through a hybrid pharmacophore- and structure-based database searching approach. *J. Med. Chem.* **2003**, *46*, 4377–92.
- (30) Ding, K.; Chen, J.; Ji, M.; Wu, X.; Varady, J.; Yang, C. Y.; Lu, Y.; Deschamps, J. R.; Levant, B.; Wang, S. Enantiomerically pure hexahydropyrazinoquinolines as potent and selective dopamine 3 subtype receptor ligands. *J. Med. Chem.* **2005**, *48*, 3171–81.
- (31) Micheli, F.; Bonanomi, G.; Braggio, S.; Capelli, A. M.; Celestini, P.; Damiani, F.; Di Fabio, R.; Donati, D.; Gagliardi, S.; Gentile, G.; Hamprecht, D.; Petrone, M.; Radicelli, S.; Tedesco, G.; Terreni, S.; Worby, A.; Heidbreder, C. New fused benzazepine as selective D3 receptor antagonists. Synthesis and biological evaluation. Part one: [h]-fused tricyclic systems. *Bioorg. Med. Chem. Lett.* **2008**, *18*, 901–7.
- (32) Palczewski, K.; Kumakawa, T.; Hori, T.; Behnke, C. A.; Motoshima, H.; Fox, B. A.; Le Trong, I.; Teller, D. C.; Okada, T.; Stenkamp, R. E.; Yamamoto, M.; Miyano, M. Crystal structure of rhodopsin: A G protein-coupled receptor. *Science* **2000**, *289*, 739–745.
- (33) Ivanov, A. A.; Barak, D.; Jacobson, K. A. Evaluation of Homology Modeling of G Protein-Coupled Receptors in Light of the A2A Adenosine Receptor Crystallographic Structure. *J. Med. Chem.* **2009**, *52*, 3284–3292.
- (34) Mustafi, D.; Palczewski, K. Topology of Class A G Protein-Coupled Receptors: Insights Gained from Crystal Structures of Rhodopsins, Adrenergic and Adenosine Receptors. *Mol. Pharmacol.* **2009**, *75*, 1–12.
- (35) Dal Ben, D.; Lambertucci, C.; Marucci, G.; Volpini, R.; Cristalli, G. Adenosine receptor modeling: what does the A2A crystal structure tell us. *Curr. Top. Med. Chem.* **2010**, *10*, 993–1018.
- (36) Simossis, V. A.; Heringa, J. PRALINE: a multiple sequence alignment toolbox that integrates homology-extended and secondary structure information. *Nucleic Acids Res.* **2005**, *33*, W289–W294, Web Server issue.
- (37) Ortore, G.; Tuccinardi, T.; Bertini, S.; Martinelli, A. A theoretical study to investigate D2DAR/D4DAR selectivity: receptor modeling and molecular docking of dopaminergic ligands. *J. Med. Chem.* **2006**, *49*, 1397–1407.
- (38) Robinson, S. W.; Jarvie, K. R.; Caron, M. G. High affinity agonist binding to the dopamine D3 receptor: chimeric receptors delineate a role for intracellular domains. *Mol. Pharmacol.* **1994**, *46*, 352–6.
- (39) Fiser, A.; Do, R. K.; Sali, A. Modeling of loops in protein structures. *Protein Sci.* **2000**, *9*, 1753–1773.
- (40) Laskowski, R. A.; MacArthur, M. W.; Moss, D. S.; Thornton, J. M. PROCHECK: a program to check the stereochemical quality of protein structures. *J. Appl. Crystallogr.* **1993**, *26*, 283–291.
- (41) Case, D. A.; Darden, T. A.; Cheatham, T. E. I.; Simmerling, C. L.; Wang, J.; Duke, R. E.; Luo, R.; Merz, K. M.; Wang, B.; Pearlman, D. A.; Crowley, M.; Brozell, S.; Tsui, V.; Gohlke, H.; Mongan, J.; Hornak, V.; Cui, G.; Beroza, P.; Schafmeister, C.; Caldwell, J. W.; Ross, W. S.; Kollman, P. A. AMBER 8; University of California, San Francisco, CA, 2004.
- (42) Martinelli, A.; Tuccinardi, T. GPCR modeling: methods and validation. An overview of recent developments. *Expert Opin. Drug Discovery* **2006**, *1*, 459–476.
- (43) Javitch, J. A.; Fu, D.; Chen, J.; Karlin, A. Mapping the binding-site crevice of the dopamine D2 receptor by the substituted-cysteine accessibility method. *Neuron* **1995**, *14*, 825–831.
- (44) Javitch, J. A.; Fu, D.; Chen, J. Residues in the Fifth Membrane-Spanning Segment of the Dopamine D2 Receptor Exposed in the Binding-Site Crevice. *Biochemistry* **1995**, *34*, 16433–16439.
- (45) Fu, D.; Ballesteros, J. A.; Weinstein, H.; Chen, J.; Javitch, J. A. Residues in the Seventh Membrane-Spanning Segment of the Dopamine D2 Receptor Accessible in the Binding-Site Crevice. *Biochemistry* **1996**, *35*, 11278–11285.
- (46) Javitch, J. A.; Ballesteros, J. A.; Weinstein, H.; Chen, J. A Cluster of Aromatic Residues in the Sixth Membrane-Spanning Segment of the Dopamine D2 Receptor Is Accessible in the Binding-Site Crevice. *Biochemistry* **1998**, *37*, 998–1006.
- (47) Javitch, J. A.; Ballesteros, J. A.; Chen, J.; Chiappa, V.; Simpson, M. M. Electrostatic and Aromatic Microdomains within the Binding-Site Crevice of the D2 Receptor: Contributions of the Second Membrane-Spanning Segment. *Biochemistry* **1999**, *38*, 7961–7968.
- (48) Javitch, J. A.; Shi, L.; Simpson, M. M.; Chen, J.; Chiappa, V.; Visiers, I.; Weinstein, H.; Ballesteros, J. A. The Fourth Transmembrane Segment of the Dopamine D2 Receptor: Accessibility in the Binding-Site Crevice and Position in the Transmembrane Bundl. *Biochemistry* **2000**, *39*, 12190–12199.
- (49) Shi, L.; Simpson, M. M.; Ballesteros, J. A.; Javitch, J. A. The First Transmembrane Segment of the Dopamine D2 Receptor: Accessibility in the Binding-Site Crevice and Position in the Transmembrane Bundle. *Biochemistry* **2001**, *40*, 12339–12348.
- (50) Shi, L.; Javitch, J. A. The second extracellular loop of the dopamine D2 receptor lines the binding-site crevice. *Proc. Natl. Acad. Sci. U.S.A.* **2004**, *101*, 440–445.
- (51) Mansour, A.; Meng, F.; Meador-Woodruff, J. H.; P., T. L.; Civelli, O.; Akil, H. Site-Directed Mutagenesis of the Human Dopamine D2 Receptor. *Eur. J. Pharmacol.* **1992**, *227*, 205–214.
- (52) Cox, B. A.; Henningssen, R. A.; Spanoynannis, A.; Neve, R. L.; Neve, K. A. Contributions of conserved serine residues to the interactions of ligands with dopamine D2 receptors. *J. Neurochem.* **1992**, *59*, 627–635.
- (53) Cho, W.; Mansour, A.; Taylor, L. P. Hydrophobic Residues of the D2 Dopamine Receptor Are Important for Binding and Signal Transduction. *J. Neurochem.* **1995**, *65*, 2105–2115.
- (54) Woodward, R.; Coley, C.; Daniell, S.; Naylor, L. H.; Strange, P. G. Investigation of the role of conserved serine residues in the long form of the rat D2 dopamine receptor using site-directed mutagenesis. *J. Neurochem.* **1996**, *66*, 394–402.
- (55) Wiens, B. L.; Nelson, C. S.; Neve, K. A. Contribution of serine residues to constitutive and agonist-induced signalling via the D2s dopamine receptor: evidence for multiple, agonist-specific active conformations. *Mol. Pharmacol.* **1998**, *54*, 435–444.
- (56) Coley, C.; Woodward, R.; Johansson, A. M.; Strange, P. G.; Naylor, L. H. Effect of multiple serine/alanine mutations in the transmembrane spanning region V of the D2 dopamine receptor on ligand binding. *J. Neurochem.* **2000**, *74*, 358–366.
- (57) Shi, L.; Javitch, J. A. The binding site of aminergic G protein-coupled receptors: the transmembrane segments and second extracellular loop. *Annu. Rev. Pharmacol. Toxicol.* **2002**, *42*, 437–467.
- (58) Ballesteros, J. A.; Shi, L.; Javitch, J. A. Structural mimicry in G protein-coupled receptors: implications of the high-resolution of rhodopsin for structure-function analysis of rhodopsin-like receptors. *Mol. Pharmacol.* **2001**, *60*, 1–19.
- (59) Sartania, N.; Strange, P. G. Role of conserved serine residues in the interaction of agonists with D3 dopamine receptors. *J. Neurochem.* **1999**, *72*, 2621–4.
- (60) Tuccinardi, T.; Ortore, G.; Manera, C.; Saccomanni, G.; Martinelli, A. Adenosine receptor modelling. A1/A2a selectivity. *Eur. J. Med. Chem.* **2006**, *41*, 321–329.
- (61) Shi, L.; Liapakis, G.; Xu, R.; Guarneri, F.; Ballesteros, J. A.; Javitch, J. A.  $\beta 2$  Adrenergic Receptor Activation: Modulation of the Proline Kink in Transmembrane 6 by a Rotamer Toggle Switch. *J. Biol. Chem.* **2002**, *277*, 40989–40996.
- (62) Lundstrom, K.; Turpin, M. P.; Large, C.; Robertson, G.; Thomas, P.; Lewell, X. Q. Mapping of dopamine D3 receptor binding site by pharmacological characterization of mutants expressed in CHO cells with the Semliki Forest virus system. *J. Recept. Signal Transduction Res.* **1998**, *18*, 133–50.
- (63) Alberts, G. L.; Pregenzer, J. F.; Im, W. B. Identification of transmembrane regions critical for ligand binding to the human D3 dopamine receptor using various D3/D1 transmembrane chimeras. *Mol. Pharmacol.* **1998**, *54*, 379–88.
- (64) Bettinetti, L.; Schlotter, K.; Hubner, H.; Gmeiner, P. Interactive SAR studies: rational discovery of super-potent and highly selective dopamine D3 receptor antagonists and partial agonists. *J. Med. Chem.* **2002**, *45*, 4594–7.
- (65) Ehrlich, K.; Gotz, A.; Bollinger, S.; Tschauder, N.; Bettinetti, L.; Harterich, S.; Hubner, H.; Lanig, H.; Gmeiner, P. Dopamine D2, D3, and D4 selective phenylpiperazines as molecular probes to explore the origins of subtype specific receptor binding. *J. Med. Chem.* **2009**, *52*, 4923–35.
- (66) Cha, M. Y.; Lee, I. Y.; Cha, J. H.; Choi, K. I.; Cho, Y. S.; Koh, H. Y.; Pae, A. N. QSAR studies on piperazinylalkylisoaxazole analogues selectively acting on dopamine D3 receptor by HQSAR and CoMFA. *Bioorg. Med. Chem.* **2003**, *11*, 1293–8.
- (67) Jones, G.; Willett, P.; Glen, R. C.; Leach, A. R.; Taylor, R. J. Development and validation of a genetic algorithm for flexible docking. *J. Mol. Biol.* **1997**, *267*, 727–748.
- (68) Chivers, J. K.; Gommeren, W.; Leysen, J. E.; Jenner, P.; Marsden, C. D. Comparison of the in-vitro receptor selectivity of substituted benzamide drugs for brain neurotransmitter receptors. *J. Pharm. Pharmacol.* **1988**, *40*, 415–421.
- (69) Millan, M. J.; Audinot, V.; Rivet, J. M.; Gobert, A.; Vian, J.; Prost, J. F.; Spedding, M.; Peglion, J. L. S 14297, a novel selective ligand at cloned human dopamine D3 receptors, blocks 7-OH-DPAT-induced hypothermia in rats. *Eur. J. Pharmacol.* **1994**, *260*, R3–5.
- (70) Sokoloff, P.; Giros, B.; Martres, M. P.; Bouthenet, M. L.; Schwartz, J. C. Molecular cloning and characterization of a novel dopamine receptor (D3) as a target for neuroleptics. *Nature* **1990**, *347*, 146–51.

- (71) Peglion, J. L.; Vian, J.; Goument, B.; Despaux, N.; Audinot, V.; Millan, M. J. Tetracyclic analogues of [+]S 14297: Synthesis and determination of affinity and selectivity at cloned human dopamine D3 vs D2 receptors. *Bioorg. Med. Chem. Lett.* **1997**, *7*, 881–886.
- (72) Zhao, Y.; Li, X.; Yang, C.; Huang, Z.; Fu, W.; Hou, T.; Zhang, J. Computational Modeling Toward Understanding Agonist Binding on Dopamine 3. *J. Chem. Inf. Model.* **2010**, *50*, 1633–1643.
- (73) Hobrath, J. V.; Wang, S. Computational elucidation of the structural basis of ligand binding to the dopamine 3 receptor through docking and homology modeling. *J. Med. Chem.* **2006**, *49*, 4470–6.
- (74) Nilsson, J.; Wikstrom, H.; Smilde, A.; Glase, S.; Pugsley, T.; Cruciani, G.; Pastor, M.; Clementi, S. GRID/GOLPE 3D quantitative structure-activity relationship study on a set of benzamides and naphthamides, with affinity for the dopamine D3 receptor subtype. *J. Med. Chem.* **1997**, *40*, 833–40.
- (75) GOLPE, version 4.5; Multivariate Infometric Analysis Srl.: Perugia, Italy, 1999.
- (76) Tuccinardi, T. Docking-Based Virtual Screening: Recent Developments. *Comb. Chem. High Throughput Screen.* **2009**, *12*, 303–314.
- (77) NCI/DTP Open Chemical Repository; National Cancer Institute: Bethesda, MD; <http://dtp.cancer.gov/> (Accessed 03/15/10).
- (78) Heidler, P.; Zohrabi-Kalantari, V.; Calmels, T.; Capet, M.; Berrebi-Bertrand, I.; Schwartz, J. C.; Stark, H.; Link, A. Parallel synthesis and dopamine D3/D2 receptor screening of novel {4-[4-(2-methoxyphenyl)piperazin-1-yl]butyl}carboxamides. *Bioorg. Med. Chem.* **2005**, *13*, 2009–14.
- (79) Leopoldo, M.; Lacivita, E.; Colabufo, N. A.; Contino, M.; Berardi, F.; Perrone, R. First structure-activity relationship study on dopamine D3 receptor agents with N-[4-(4-arylpirperazin-1-yl)butyl]arylcaboxamide structure. *J. Med. Chem.* **2005**, *48*, 7919–22.
- (80) Wustrow, D.; Belliotti, T.; Glase, S.; Kesten, S. R.; Johnson, D.; Colbry, N.; Rubin, R.; Blackburn, A.; Akunne, H.; Corbin, A.; Davis, M. D.; Georgic, L.; Whetzel, S.; Zoski, K.; Heffner, T.; Pugsley, T.; Wise, L. Aminopyrimidines with high affinity for both serotonin and dopamine receptors. *J. Med. Chem.* **1998**, *41*, 760–71.
- (81) Boeckler, F.; Gmeiner, P. The structural evolution of dopamine D3 receptor ligands: structure-activity relationships and selected neuropharmacological aspects. *Pharmacol. Ther.* **2006**, *112*, 281–333.
- (82) Belliotti, T. R.; Kesten, S. R.; Wustrow, D. J.; Georgic, L. M.; Zoski, K. T.; Akunne, H. C.; Wise, L. D. Novel cyclohexyl amides as potent and selective D3 dopamine receptor ligands. *Bioorg. Med. Chem. Lett.* **1997**, *7*, 2403–2408.
- (83) Murray, A. M.; Hyde, T. M.; Knable, M. B.; Herman, M. M.; Bigelow, L. B.; Carter, J. M.; Weinberger, D. R.; Kleinman, J. E. Distribution of putative D4 dopamine receptors in postmortem striatum from patients with schizophrenia. *J. Neurosci.* **1995**, *15*, 2186–91.
- (84) Gasteiger, E.; Gattiker, A.; Hoogland, C.; Ivanyi, I.; Appel, R. D.; Bairoch, A. ExPASy: the proteomics server for in-depth protein knowledge and analysis. *Nucleic Acids Res.* **2003**, *31*, 3784–3788.
- (85) Palczewski, K.; Kumadasaka, T.; Hori, T.; Behnke, C. A.; Motoshima, H.; Fox, B. A.; Le Trong, I.; Teller, D. C.; Okada, T.; Stenkamp, R. E.; Yamamoto, M.; Miyano, M. Crystal structure of rhodopsin: a G-protein-coupled receptor. *Science* **2000**, *289*, 739–745.
- (86) Berman, H. M.; Westbrook, J.; Feng, Z.; Gilliland, G.; Bhat, T. N.; Weissig, H.; Shindyalov, I. N.; P.E., B. The Protein Data Bank. *Nucleic Acids Res.* **2000**, *28*, 235–242.
- (87) McGuffin, L. J.; Bryson, K.; Jones, D. T. The PSIPRED protein structure prediction server. *Bioinformatics* **2000**, *16*, 404–405.
- (88) Ballesteros, J. A.; Weinstein, H. W. Integrated methods for the construction of three-dimensional models and computational probing of structure-function relations in G-protein coupled receptors. *Methods Neurosci.* **1995**, *25*, 366–428.
- (89) Tuccinardi, T.; Calderone, V.; Rapposelli, S.; Martinelli, A. Proposal of a New Binding Orientation for Non-Peptide AT1 Antagonists: Homology Modeling, Docking and Three-Dimensional Quantitative Structure-Activity Relationship Analysis. *J. Med. Chem.* **2006**, *49*, 4305–4316.
- (90) Jakalian, A.; Jack, D. B.; Bayly, C. I. Fast, efficient generation of high-quality atomic charges. AM1-BCC model: II. Parameterization and validation. *J. Comput. Chem.* **2002**, *23*, 1623–1641.
- (91) Maestro, version 7.5; Schrödinger Inc.: Portland, OR, 1999.
- (92) Macromodel , version 8.5; Schrödinger Inc.: Portland, OR, 1999.
- (93) Goodford, P. J. A computational procedure for determining energetically favorable binding sites on biologically important macromolecules. *J. Med. Chem.* **1985**, *28*, 849–857.
- (94) Tuccinardi, T.; Ortore, G.; Rossello, A.; Supuran, C. T.; Martinelli, A. Homology Modeling and Receptor-Based 3D-QSAR Study of Carbonic Anhydrase IX. *J. Chem. Inf. Model.* **2007**, *47*, 2253–2262.
- (95) Petersen, E. F.; Goddard, T. D.; Huang, C. C.; Couch, G. S.; Greenblatt, D. M.; Meng, E. C.; Ferrin, T. E. UCSF Chimera--a visualization system for exploratory research and analysis. *J. Comput. Chem.* **2004**, *25*, 1605–1612.
- (96) Freedman, S. B.; Patel, S.; Marwood, R.; Emms, F.; Seabrook, G. R.; Knowles, M. R.; McAllister, G. Expression and pharmacological characterization of the human D3 dopamine receptor. *J. Pharmacol. Exp. Ther.* **1994**, *268*, 417–426.

CI100290F